Biochemical Characterization and Electron-Transfer Reactions of *syml*, a *Rhodobacter capsulatus* Reaction Center Symmetry Mutant Which Affects the Initial Electron Donor†

Aileen K. W. Taguchi,‡ Jonathan W. Stocker,§ Rhett G. Alden,‡ Timothy P. Causgrove,‡ Jeffrey M. Peloquin,‡ Steven G. Boxer,*,§ and Neal W. Woodbury*,‡

Department of Chemistry and Biochemistry and Center for the Study of Early Events in Photosynthesis, Arizona State University, Tempe, Arizona 85287-1604, and Department of Chemistry, Stanford University, Stanford, California 94305-5080

Received January 27, 1992; Revised Manuscript Received July 16, 1992

ABSTRACT: A 51 bp section of the *Rhodobacter capsulatus* photosynthetic reaction center M subunit gene (nucleotides M562–M612 of the *pufM* structural sequence) encoding amino acids M187–M203 was replaced by the homologous region of the L subunit gene. This resulted in the symmetrization of much of the amino acid environment of the reaction center initial electron donor, P. This is the first in a series of large-scale symmetry mutations and is referred to as *syml*. The *syml* mutant was able to grow photosynthetically, indicating that reaction center function was largely intact. Isolated reaction centers showed an approximately 10-nm blue shift in the Q_Y band of P. The standard free energy change between P* and $P^+Bph_A^-$ determined from analysis of the long-lived fluorescence from quinone-reduced reaction centers decreased from about −120 meV in the wild-type to about −75 meV in the *syml* mutant. A 65–70% quantum yield of electron transfer from P* to $P^+Q_A^-$ was observed, most of the yield loss occurring between P* and $P^+Bph_A^-$. The decay of the stimulated emission from P* was about 3-fold slower in this mutant than in the wild-type. Time-resolved spectral analysis of the charge-separated intermediates formed in *syml* reaction centers indicated that the major product was $P^+Bph_A^-$. A model-dependent analysis of the observed rates and electron-transfer yields gave the following microscopic rate constants for *syml* reaction centers (wild-type values under the same conditions are given in parentheses):

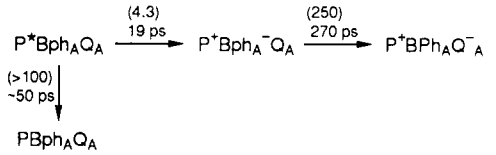

Analysis of the *syml* mutant, mutants near P made by other groups, and interspecies variation of amino acids in the vicinity of P suggests that the protein asymmetry in the environment of the initial electron donor is important for optimizing the rate and yield of electron transfer, but is not strictly required for overall reaction center function.

One of the most interesting aspects of the structure of the photosynthetic bacterial reaction center is its approximate C_2 symmetry (Deisenhofer et al., 1984; Allen et al., 1987; Chang et al., 1991). Though the symmetry extends throughout the reaction center core structure, it is most striking at the level of the cofactors. Two bacteriochlorophylls (Bch) interact to form a dimer which serves as the initial electron donor (P). P is situated near the periplasmic side of the integral membrane reaction center complex. Progressing toward the cytoplasmic side, there are two monomer Bchs (Bch_A and Bch_B), two bacteriopheophytins (Bph_A and Bph_B), and two quinones (Q_A and Q_B). These two sets of redox-active cofactors are placed symmetrically about a transmembrane rotational axis forming two potential pathways for electron transfer ($P \rightarrow Bch_A \rightarrow Bph_A \rightarrow Q_A$ and $P \rightarrow Bch_B \rightarrow Bph_B \rightarrow Q_B$). The relative distances and orientations of the cofactors which make up the two pathways are very similar.

The apparent similarity of the two electron-transfer pathways is deceptive, however, since transient spectroscopic studies have shown that electron transfer is essentially unidirectional, proceeding down the A pathway. Light initiates these reactions by forming the excited singlet state of P, P*. Electron transfer occurs, forming the state $P^+Bph_A^-$ within about 3.5 ps. (The role of Bch_A and that of its anion in this reaction are presently a subject of debate.) The electron then proceeds from Bph_A to Q_A in about 200 ps and finally from Q_A to Q_B in about 200 μs [reviewed by Kirmaier and Holten (1987) and Feher et al. (1989)].

It is not clear at this point whether the functional asymmetry is due completely to the small differences in the relative positions and orientations of the cofactors, or whether the

† N.W.W., A.K.W.T., and S.G.B. acknowledge support from the NSF Biophysics program. N.W.W. performed part of this work as an NSF Plant Molecular Biology Postdoctoral Fellow. J.W.S. is an NSF Predoctoral Fellow. R.G.A. is an NSF Postdoctoral Fellow in Plant Biology. This work utilized instrumentation purchased with funds from NSF Grant DIR 8804992 (NSF Biological Centers Program) and DOE Instrumentation Grants DE-FG05-88ER75443 and DE-FG05-87ER75361 (University Research Instrumentation Program). This is Publication No. 104 from the Arizona State University Center for the Study of Early Events in Photosynthesis. The Center is funded by U.S. Department of Energy Grant DE-FG02-88ER13969 as part of the USDA/DOE/NSF Plant Science Centers program.

* To whom correspondence should be addressed.
‡ Arizona State University.
§ Stanford University.

0006-2960/92/0431-10345$03.00/0

much greater asymmetry of the protein environment surrounding the cofactors plays a major role. The asymmetry in the position and the environment of the cofactors is also ultimately due to the protein asymmetry, since the protein both holds these molecules in place and defines the environment in which the redox chemistry occurs.

The availability of two structurally similar but functionally distinct electron-transfer pathways within the reaction center provides an excellent system for the study of protein effects on electron-transfer reactions. If one could understand how the protein environment differentially modulates the thermodynamic and kinetic properties of electron transfer between the two pathways, a great deal would be learned about protein–cofactor interactions in general, particularly as they pertain to electron-transfer reactions. We have chosen to probe the differences between the protein environments of the two potential electron-transfer pathways by symmetrizing the reaction center subunits: using genetic manipulation to replace DNA sequences from one core subunit gene with homologous sequences from the other. The resulting reaction centers are then subjected to a series of biophysical analyses to determine the kinetic and thermodynamic parameters of electron transfer as well as to characterize the states involved.

Systems for performing genetic manipulations of these subunits have been developed (Youvan et al., 1985; Paddock et al., 1989; Farchaus & Oesterhelt, 1989; Nagarajan et al., 1990; Takahashi et al., 1990) and have resulted in a number of recent publications on site-directed mutants [e.g., Bylina et al. (1988a,b), Kirmaier et al. (1988), Paddock et al. (1989), Finkele et al. (1990), Hammes et al. (1990), Middendorf et al. (1991), Nagarajan et al. (1990), Takahashi et al. (1990), Williams et al. (1992), Kirmaier et al. (1991), and Chan et al. (1991)]. The most ambitious attempt at symmetrization thus far was performed by Robles et al. (1990). In one of these mutants, almost the entire D helix of M was replaced by L sequences. The reaction centers from this mutant were unstable to isolation and showed little or no electron-transfer activity in membranes, apparently because Bph_A is lost. However, single-site revertants were isolated which showed clear photosynthetic function, though complete characterization of the electron-transfer reactions has not yet been reported.

In this report, we describe the construction and characterization of *syml*, the first in a series of large-scale symmetry mutants. Rather than using protein secondary structural units (such as transmembrane helices) as a guide to determining the regions to symmetrize, we have chosen to define our mutated regions by the cofactors they most strongly affect. The mutant described here involves symmetrization of a large fraction of the environment of the initial electron donor, P. The resulting reaction centers are photosynthetically active. Extensive characterization of these reaction centers has been performed and has been presented in this and the following paper (Stocker et al., 1992). A preliminary report of this work was published previously (Woodbury et al., 1990).

MATERIALS AND METHODS

Plasmid Constructions. The *pufM* gene was subcloned on a *Kpn*I–*Bam*HI endonuclease fragment from pU29 (Bylina et al., 1986) into a derivative of pBR322. A 55-base oligonucleotide and a 53-base oligonucleotide were synthesized to replace bases M562–M612 (amino acids M187–M203) of *pufM* with the homologous *pufL* sequences, bases L481–L531 (amino acids L160–L176). The annealed oligonucleotides were used to replace an *Xmn*I–*Pvu*I restriction endonuclease fragment in the pBR322 derivative containing the *pufM* gene. DNA sequencing of one strand with Sequenase Version 2.0 (U.S. Biochemical Corp.) confirmed correct insertion of the oligonucleotides, and no alterations were detected in the adjacent 150 bp of flanking sequences. The gene construct was cloned into pCR (plasmid for conjugation and replication, which will be described elsewhere), a derivative of pU2922 (Youvan et al., 1985; Bylina et al., 1986). pU2922 and pU29 were generously provided by Professor Douglas Youvan. For the purposes of this report, the *puf* operon sequences of either pU2922 or pU29 are considered to be wild-type, though both contain silent mutations in structural gene sequences (Youvan et al., 1985; Bylina et al., 1986). The final plasmid, pAT-3, was transformed into *Escherichia coli* strain S17-1 (Simon et al., 1983) and transconjugated into U43, a deletion strain of *Rhodobacter capsulatus* (*Rb. capsulatus*) lacking most of the *puf* operon and containing a point mutation which eliminates the B800/B850 bacteriochlorophylls from the photosynthetic membrane (Youvan et al., 1985). The resulting reaction centers contain a substitution of 17 amino acids of the M protein with 17 amino acids from the L protein (Figure 1A). Nine of these seventeen amino acids differ between the two subunits. *pufL* and its gene product were unchanged.

Chromatophore and Reaction Center Isolation. Wild-type and *syml* reaction centers were isolated from U43 transconjugants containing pU2922 or pAT-3 [procedure modified from Prince and Youvan (1987) and described below]. U43 transconjugants containing either plasmid pAT-3 or pU2922 were grown by diluting (1:100) a dark grown inoculum of cells into 2 L of YCC/kan medium (0.5% Difco yeast extract, 0.6% Difco casamino acids, 0.00355% ethylenediaminetetraacetic acid tetrasodium salt, 0.00002% $CuSO_4 \cdot 5H_2O$, 0.000015% $CoCl_2 \cdot 6H_2O$, 0.00125% nitrilotriacetic acid, 0.00001% $(NH_4)_6Mo_7O_{24} \cdot 4H_2O$, 0.02% $MgSO_4 \cdot 7H_2O$, 0.000375% $FeSO_4 \cdot 7H_2O$, 0.00000625% H_3BO_3, 0.00345% $Ca(NO_3)_2 \cdot 4H_2O$, pH 7.2, 15 μg/mL kanamycin) in a 2.8-L Fernbach flask. Cultures were shaken in the dark at 200 rpm in a New Brunswick air shaker for 3 days at 32 °C. The cells were harvested by low-speed centrifugation, resuspended in a minimal amount of 10 mM potassium phosphate, pH 7.35, lysed using a French pressure cell at 20 000 psi, recentrifuged at low speed to remove uncracked cells and large cell debris, and finally ultracentrifuged in a Ti 50.2 rotor at 45 000 rpm for 90 min to pellet the chromatophores (photosynthetic membranes). To isolate reaction centers, chromatophores were resuspended to an optical density of about 25 at 875 nm in washing buffer (10 mM potassium phosphate, pH 7.35, 0.05% LDAO). (LDAO was generously provided by Stepan Co., Millsdale Works, Elwood, IL.) LDAO was added to a final concentration of 1.5%, and the sample was incubated at 37 °C for 10 min and then placed on ice. Approximately 1/5 volume of DEAE-Sephacel (Pharmacia) was added to the solubilized material and slowly mixed for 5 min. This was then allowed to settle, and the unbound material was drained off and mixed with another 1/5 volume of DEAE. The two DEAE samples were added together, and this was washed by repeated mixing and decanting in washing buffer. Finally, a column was prepared using fresh DEAE for the bottom half of the bed and DEAE bound to the solubilized reaction centers for the top half. Reaction centers were eluted with a salt gradient (50–300 mM KCl in washing buffer) after washing the column extensively with phosphate buffer containing 0.05–0.6% LDAO, depending on the preparation. Reaction centers purified in this way are not as pure as can be obtained by other

methods (Prince & Youvan, 1987). The OD_{280}/OD_{800} ratio is typically 2.0–2.5. However, the yield is considerably higher using this technique, and in our experience, some mutant reaction centers, including the one described here, tend to be difficult to isolate with yields high enough to easily perform detailed fast spectroscopy using other methods. We have also isolated reaction centers from this mutant using standard techniques (Prince & Youvan, 1987) and obtained higher purity (OD_{280}/OD_{800} = 1.4), and the steady-state optical properties, recombination kinetics, and yield of photochemistry were all essentially unaltered.

Steady-State Spectroscopy. Steady-state spectra were taken with a Cary-5 spectrometer (Varian Instruments). For light-minus-dark difference spectra, the samples were illuminated at 90° with a 1000-W lamp set at 30% power through a water filter and a BG39 blue filter (Corning). A RG630 filter (Corning) was used to block actinic light from entering the detector.

Measurements of $P^+Q_A^-$ Quantum Yields. Quantum yields of $P^+Q_A^-$ formation were measured with a home-built flash spectrometer. The actinic source was a flash lamp pumped-dye laser with a roughly 500-ns pulse length at 600 nm. The light intensities were varied with calibrated neutral density filters.

Time-Correlated Single-Photon Counting. The time-correlated single-photon counting apparatus has been described previously (Gust et al., 1990). For this work, approximately 10-ps excitation pulses at 3.8 MHz from a cavity-dumped, synchronously-pumped, styryl-9 dye laser at 860 nm (Spectra Physics) were used. The dye laser was pumped by an Antares mode-locked Nd-YAG laser (Coherent). For quinone-reduced reaction centers, approximately 50–100 mW/cm^2 excitation light was used. The emission was passed through a 0.25-m subtractive monochromator (Instruments SA) with a spectral bandwidth of ±8 nm. The emission was detected by a microchannel plate photomultiplier tube with an S1 photocathode (Hamamatsu) for enhanced near-infrared sensitivity. The timing circuitry and analysis software have been described (Gust et al., 1990). The full width at half-maximum of the instrument response function (light scattered from a LUDOX suspension at the excitation wavelength) was 70–90 ps.

Subpicosecond Resolution Transient Absorption Spectroscopy. A pump–probe transient absorption apparatus was utilized to measure the spectral and kinetic characteristics of the early states involved in charge separation. The short laser pulses were generated by a dye laser synchronously pumped by a frequency-doubled, mode-locked Nd-YAG laser (Spectra Physics). Both the Nd-YAG laser pulse train and the dye laser pulse train were compressed by fiber pulse compressors (Spectra Physics). The final pulse output was a 590-nm, 80-fs, 0.5-nJ pulse. This pulse was amplified in a three-stage pulse amplifier pumped by a frequency-doubled (532 nm), 540-Hz repetition rate, 10-mJ regeneratively amplified (Continuum) Nd-YAG pulse seeded by the mode-locked Nd-YAG laser. The output of the dye amplifier was a roughly 200-μJ, 590-nm pulse with a pulse duration of approximately 150 fs. This pulse was split into two parts (about 60% for the probe pulse, 40% for the excitation pulse). The excitation beam was passed through appropriate neutral density filters and used to excite a roughly 2-mm^2 area of the sample. The probe beam was passed through a variable optical delay, focused into a 1 cm wide flowing water cell for continuum generation, and filtered to select the spectral region to probe and to reduce the intensity to the desired level. The probe pulse was then split into two equal parts. One part was passed through the excited region of the sample. The other half was passed through an unexcited region. Each pulse was then focused onto one branch of a bifurcated fiber optic bundle (Princeton Instruments) which was optically coupled into an 0.275-m monochromator (Acton Research). The exit slit of the monochromator was removed and replaced by a dual diode array detector (Princeton Instruments). The delay line position, monochromator wavelength, and data collection were controlled via a combination of locally written software in a LabWindows (National Instruments) environment and software for the dual diode array system provided by the manufacturer. For all experiments reported, each time scan consisted of 100 spectra at different times, each encompassing a 140-nm region. Data were averaged for 2 s (1080 shots) per time point.

In order to avoid accumulation of the state P^+ in the reaction center samples, a rotating circular cuvette was utilized. The cuvette had a 3-mm path length and a circumference of 50 cm. It rotated at about 2 Hz. The total sample volume was 3–4 mL. This is rapid enough so that the excited region of the sample is removed completely between pulses. The pulse energies used in these experiments were approximately 5 μJ/pulse [about 250 μJ/(cm^2·pulse)]. For these experiments all excitation was performed at 590 nm, and absorption changes in the 840–860-nm region (the Q_Y band of P) were always less than or equal to 20% of the total absorption in that wavelength region. In all experiments reported here, the relative polarization of the probe and excitation pulses was at the magic angle.

RESULTS

Construction. Figure 1A shows the detailed changes between the wild-type and *syml pufM* gene and gene product. Of the roughly 11 amino acids in the M subunit that come in close contact with the reaction center initial electron donor, 5 fall within the segment exchanged (Yeates et al., 1988; El-Kabbani et al., 1991). Figure 1B shows the structure of the *Rhodobacter sphaeroides* (*Rb. sphaeroides*) reaction center L and M sequences which are homologous to the *Rb. capsulatus* sequences symmetrized in this mutant. In addition, the relative positions and orientations of P and the monomer Bchs are shown (Allen et al., 1987). This region in both the L and M subunits includes a small segment of the C/D interhelix region and the top of the D helix. Homology between the primary amino acid sequences of *Rb. capsulatus* and *Rb. sphaeroides* is very high in this region (≥80%). Thus, the *Rb. sphaeroides* structure near P is probably a reasonable model for structural comparison with *Rb. capsulatus*.

Photosynthetic Viability of the syml Mutant. Early log-phase transconjugants of U43 containing pU2922 (which contains the wild-type *puf* operon) and of U43 containing pAT-3 (which contains the *syml* mutation) were diluted and plated on MPYE/kan (0.3% Difco Bacto-peptone, 0.3% Difco yeast extract, 1.6 mM $MgCl_2$, 1.0 mM $CaCl_2$, 1.5% agar, 15 μg/mL kanamycin) plates. Three plates of each strain were incubated in the dark at 32 °C under aerobic conditions, three in the dark at 32 °C under anaerobic conditions, and three were incubated in the light at 32 °C under anaerobic conditions. Table I presents the average number of colonies per plate for each of the three conditions. There is no significant difference between the number of colonies which grew aerobically in the dark and the number which grew anaerobically in the light, indicating that all cells in the culture are capable of photosynthetic growth.

Spectral Properties of Isolated Photosynthetic Membranes. The solid lines in Figure 2 show the near-infrared optical

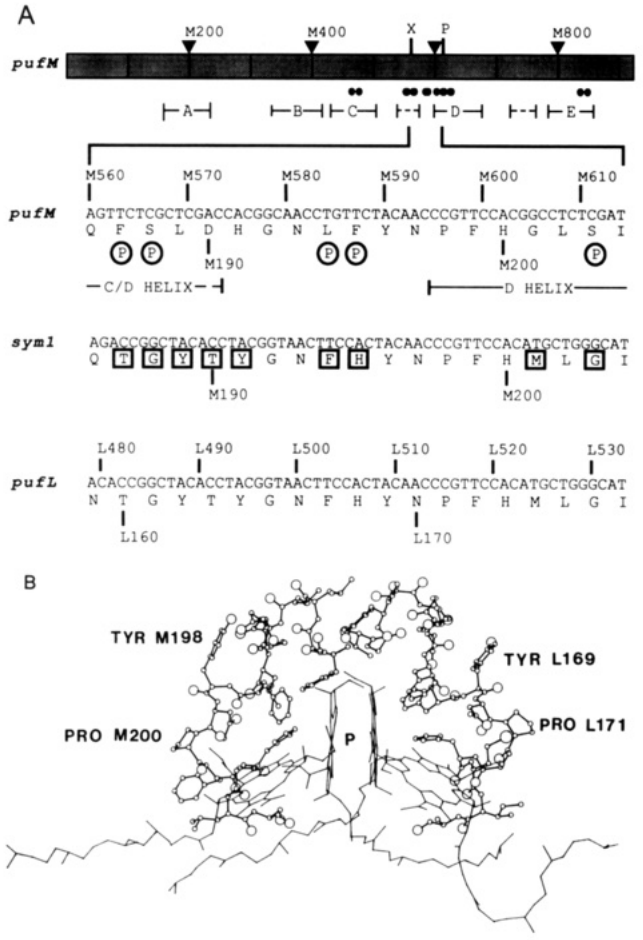

FIGURE 1: (A) The stippled bar represents the physical map of the *pufM* gene (X = *Xmn*I, P = *Pvu*I). The filled ovals below the physical map indicate regions of the gene which code for points of close contact with P in the *Rb. sphaeroides* structure (Yeates et al., 1988; El-Kabbani et al., 1991). Also shown below the physical map are the location of sequences encoding the A–E helices. In addition, the small α-helical sections between the C and D and the D and E helices are shown with dashed lines. The DNA sequences of the *Xmn*I–*Pvu*I restriction fragment from *pufM* replaced in the *syml* mutation is shown. The corresponding amino acid sequence is given below the DNA sequence. The circled "P"s mark amino acids which come in close contact with P in the *Rb. sphaeroides* structure (Yeates et al., 1988; El-Kabbani et al., 1991). DNA and amino acid sequences of the *syml* mutation and the *pufL* gene are also shown. Amino acids which differ between the *syml* mutant and the wild-type M sequence are boxed in the *syml* amino acid sequence. (B) *Rb. sphaeroides* reaction center structure of the regions homologous to the symmetry-related L and M sequences of *Rb. capsulatus* shown in (A) (Brookhaven Data Base, file 1RCR). Also shown is the special pair (labeled "P") and the two monomer Bchs (unlabeled). The symmetrically conserved amino acid pairs Tyr M198 and L169 and Pro M200 and L171 of the displayed peptide fragment are labeled for reference. (Note: M198 and M200 in *Rb. sphaeroides* correspond to M196 and M198 in *Rb. capsulatus*. The *Rb. capsulatus* numbering system for the M subunit used in part A of this figure is offset by 2 from the *Rb. sphaeroides* numbering system used in part B. The numbering of the L amino acids is the same in both species.)

spectra of chromatophores isolated from U43 expressing either wild-type or *syml* reaction centers. U43 has a point mutation which results in loss of the B800/B850 antenna complex. Thus, the only transitions observed in this region are due to the B875 antenna complex and the reaction center. In particular, the 760- and 800-nm bands are predominantly due to reaction center absorption while the 880-nm band is mostly due to antenna absorption. The ratio between the 880- and 800-nm bands is similar in the mutant and wild-type samples, indicating that the relative level of reaction center Bch to antenna Bch is similar in both strains.

Table I: Photosynthetic Viability

strain	colonies per plate		
	$+O_2$/dark	$-O_2$/dark	$-O_2$/light[a]
wild-type[b]	378 ± 56	0	315 ± 31
syml[c]	574 ± 42	0	570 ± 72

[a] Plates were illuminated with six 60-W Sylvania Lumiline incandescent bulbs about 1 ft away. [b] Aerobically grown cells were incubated for 2 days in the dark. Anaerobically grown cells were incubated for 6–7 days. Colony size for aerobically grown cells was 1 mm; for anaerobically grown cells in the light it ranged from 1 to 4 mm. [c] Aerobically grown cells were incubated for 2 days in the dark. Anaerobically grown cells were incubated for 12 days. Aerobically grown colonies were about 1 mm in diameter; light, anaerobically grown colonies ranged in size from <1 mm up to several millimeters.

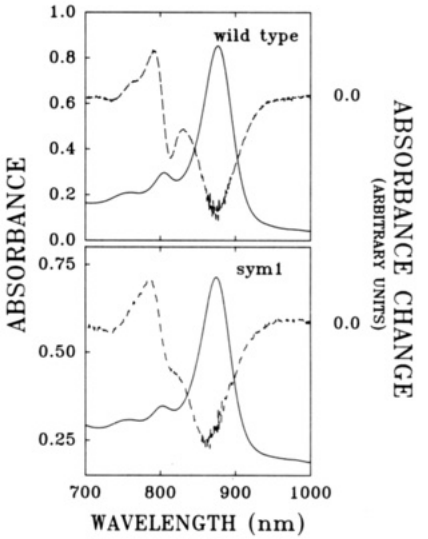

FIGURE 2: Ground-state (solid line) and light-minus-dark optical difference (dashed line) spectra of wild-type and *syml* chromatophore preparations in the near-infrared. All measurements were performed at room temperature on a Cary-5 spectrometer (Varian) modified to accept the input of an actinic light source via a fiber optic cable. The maximum absorbance changes near 875 nm upon actinic illumination were about 0.01 for both samples. This was significantly lower than the total change with saturating actinic light. Continuous saturating illumination resulted in additional, largely irreversible changes to the red of the major 875-nm bleaching.

Light-minus-dark difference spectra for wild-type and *syml* chromatophores are shown as dashed lines in Figure 2. There are several apparent differences between these spectra. First, the peak of the bleaching of the Q_Y band of P upon P^+ formation is shifted approximately 10–15 nm to higher energy in the *syml* mutant. There is also a change in the shape and magnitude of the 790- and 810-nm absorption changes that accompany P^+ formation. The cation band at 1250 nm is shifted to about 1240 nm in the mutant (data not shown, but see below for reaction centers). In addition, there is a roughly 4-fold decrease in the extinction coefficient of the 1240-nm band of *syml* relative to the corresponding wild-type band.

Biochemical and Spectral Properties of Isolated Reaction Centers. Isolation of *syml* reaction centers can be performed using essentially the same procedures as used for wild-type reaction centers (see Materials and Methods). In reaction centers, as in chromatophores, the Q_Y transition of P is 10–15 nm blue-shifted in *syml* relative to wild-type (Figure 3A,B, solid lines). In both wild-type and *syml* reaction centers, the position of this band is blue-shifted by 10–15 nm compared to the position of the corresponding bleaching observed in light-minus-dark difference spectra of chromatophores (Figure 2).

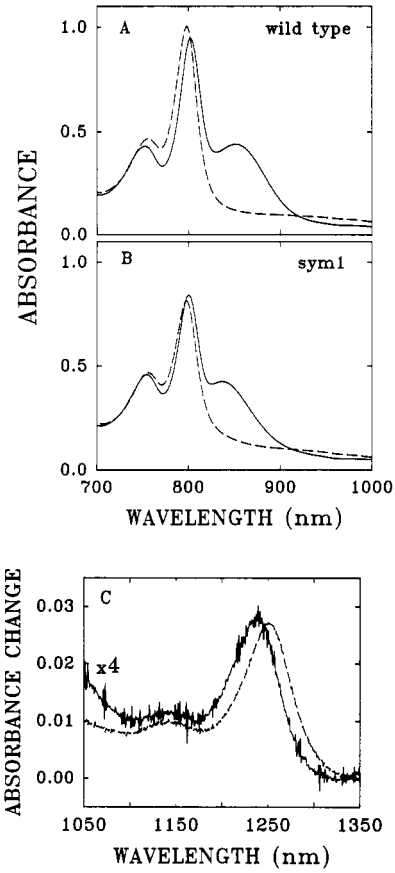

FIGURE 3: Wild-type and *syml* reaction center spectra in the presence and absence of saturating actinic illumination. (A and B) The solid lines represent the ground-state spectra; the dashed lines represent the spectrum after illumination. (C) Spectra of wild-type (dashed) and *syml* (solid) reaction centers in the 1250-nm region upon exposure to saturating actinic illumination. The scale of the absorbance change for the *syml* spectrum has been expanded by a factor of 4; for identical 860-nm bleachings, the wild-type and mutant differ in the oscillator strength of the 1250-nm band by approximately this factor.

Upon saturating illumination, the Q_Y band of P in wild-type reaction centers is completely bleached and the 800-nm band appears to shift slightly to the blue. In the *syml* mutant, one also finds complete bleaching of P's Q_Y band upon illumination and a similar, but smaller, blue shift of the 800-nm band. This is shown in Figure 3A,B as dashed lines. Figure 3C shows the absorbance increase in the 1250-nm region upon light-induced formation of P^+. This band shifts by about 10 nm to the blue in the mutant and has a roughly 4-fold lower extinction coefficient, much as was described above for chromatophores.

Pigment Composition of Mutant Reaction Centers. There is no indication from the absorbance spectrum of isolated *syml* reaction centers that the number of Bch or Bph molecules has been altered (Figure 3). Pigment extractions confirmed this expectation. Extraction of the Bchs and Bphs into acetone/methanol as described by van der Rest and Gingras (1974) resulted in a total of 6 Bphs and Bchs per mutant reaction center and a Bch to Bph ratio of 1.9 ± 0.1. These numbers are identical to control extractions performed on wild-type reaction centers.

Time-Resolved Fluorescence Decay Measurements. The bulk of the fluorescence from wild-type reaction centers decays rapidly due to quenching by electron transfer. The state $P^+Bph_A^-$ which forms from P* in picoseconds can undergo back electron transfer to re-form P* on longer time scales. If electron transfer from Bph_A to Q_A is blocked by reduction of the reaction center quinones. $P^+Bph_A^-$ lives for nanoseconds, and a substantial amount of the total fluorescence from the system comes from the long-lived residual excited singlet state that arises due to back reactions from $P^+Bph_A^-$ re-forming P* (Schenck et al., 1982). The relative amount of the long-lived fluorescence is thought to reflect the equilibrium constant between P* and $P^+Bph_A^-$ (Schenck et al., 1982; Woodbury et al., 1984).

Table II: Time-Resolved Fluorescence Decay[a]

sample[b]	A_1	τ_1 (ps)	A_2	τ_2 (ps)	A_3	τ_3 (ps)	A_4	τ_4 (ps)
w.t. RCs	98.0	9.9	1.6	100	0.27	710	0.15	5200
syml RCs	89.2	29	7.58	180	2.69	820	0.529	3400

[a] A_i and τ_i are the initial amplitudes and decay times determined from fitting the time-correlated single-photon counting traces to the sum of four exponential components, $A_1 \exp(-t/\tau_1) + A_2 \exp(-t/\tau_2) + A_3 \exp(-t/\tau_3) + A_4 \exp(-t/\tau_4)$, convoluted with the measured instrument response function. The decay amplitudes (A_1, A_2, A_3, A_4) have been normalized so that their sum is 100. The run-to-run variation in τ_1 is about ±5%; the run-to-run variation in τ_2, τ_3, and τ_4 is ±20%. A_1 varies by ±1% in wild-type samples and by ±5% in *syml* reaction centers. A_2, A_3, and A_4 vary by ±20% in all samples. [b] Reaction center quinones were reduced by adding buffered dithionite to a final concentration of 1 mM.

Table II gives the results of fluorescence decay measurements in wild-type (w.t.) and *syml* isolated reaction centers (RCs) with reduced quinones. The decay time for the initial or prompt fluorescence component, τ_1, represents the decay of the initial excited singlet state due to fast charge separation ($P^* \rightarrow P^+Bph_A^-$). This component is faster than the time resolution of our apparatus (~10 ps) for wild-type reaction centers. For *syml* reaction centers, the observed lifetime probably represents an accurate overall lifetime of fluorescence emitted during the first 50 ps (i.e., we would be unlikely to be able to accurately resolve two lifetimes less than 50 ps). A significant decrease in the rate of quenching of the initial excited singlet state is seen when comparing wild-type and *syml* reaction centers (about 10 ps for the wild-type and 29 ps for *syml*, Table II). This implies a decrease in the rate constant for the initial electron-transfer reaction in *syml* reaction centers, in qualitative agreement with ultrafast transient absorption measurements (see below).

The remaining fluorescence components (τ_2, τ_3, τ_4) in quinone-reduced samples are presumably due to back electron transfer from $P^+Bph_A^-$ re-forming P*. The complexity of the kinetic decay of the long-lived fluorescence in quinone-reduced reaction centers has been discussed previously. One reasonable hypothesis is that the free energy of the state $P^+Bph_A^-$ relaxes as a function of time (Woodbury & Parson, 1984, 1986; Sebban & Moya, 1983). The somewhat shorter value of τ_4 observed here compared to previous work is due to the shorter time range of data collection used in order to resolve the faster components accurately. Measurements made on longer time scales give values for this decay component comparable to previously published values.

Figure 4 shows the decay-associated spectra of the kinetic components of the fluorescence from quinone-reduced *syml* reaction centers. The 180-ps component has the same spectrum as the prompt fluorescence. The 820-ps component apparently includes some additional fluorescence between 880 and 900 nm which is not present in the prompt fluorescence spectrum and probably indicates slight contamination by an emitter other than P*. The longest-lived component again has a spectrum which matches that of the prompt fluorescence. Similar spectra were obtained for wild-type reaction centers (data not shown) except that the initial amplitudes of the long-lived components are much smaller (Table II).

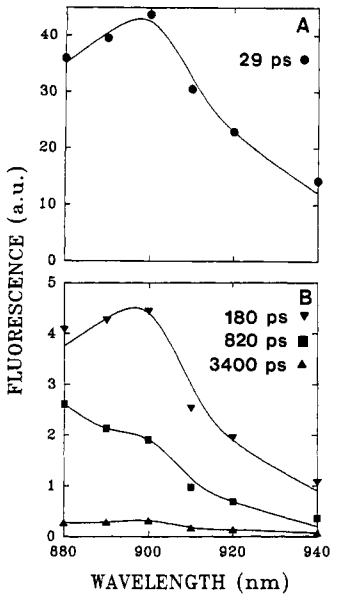

FIGURE 4: Fluorescence decay-associated spectra for quinone-reduced (Q_A^-) *syml* reaction centers. (A) Spectrum of the prompt (29-ps) fluorescence component. (B) Spectra of the three long-lived fluorescence components (180, 820, and 3400 ps). The fluorescence intensity scale for the lower panel has been expanded by about a factor of 8 relative to the top panel. Excitation was at 860 nm. Experimental conditions as described in Materials and Methods and in the footnotes to Table II. The decay-associated spectra are not corrected for the variation in photomultiplier sensitivity with wavelength.

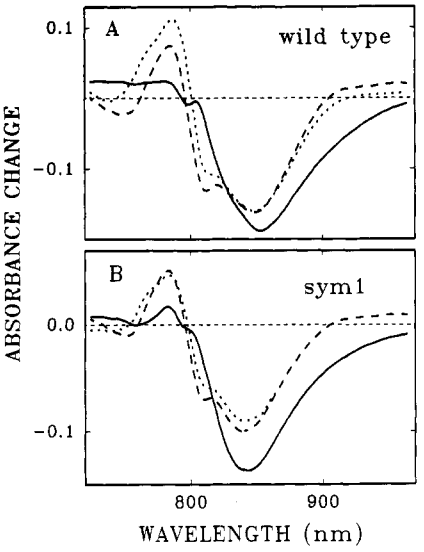

FIGURE 5: Comparison of transient difference absorption spectra for wild-type and *syml* reaction centers. Spectra were taken with a dual diode array system in two spectral regions centered at 800 nm and at 900 nm. The two spectral regions were joined by normalizing at 840 nm. (A) Wild-type reaction centers; the solid line represents spectral changes at 0.5 ps, the dashed line at 48 ps, and the dotted line at 640 ps. (B) *syml* reaction centers; the solid line represents spectral changes at 0.8 ps, the dashed line at 48 ps, and the dotted line at 640 ps.

Transient Absorption Measurements of Electron-Transfer Rates and Spectra of Intermediate States. Figure 5 shows time-resolved difference absorption spectra between 730 and 960 nm of wild-type and *syml* reaction centers. At early times (0.5 ps, wild-type; 0.8 ps, *syml*), the absorption changes are primarily due to P*. The wild-type P* spectrum shown is in good agreement with previous reports (Kirmaier & Holten, 1988). Other than the shift in the position of the bleaching of the Q_Y band of P, there is little difference between the P* spectra of wild-type and *syml* reaction centers.

In wild-type reaction centers, absorption changes recorded 48 ps after excitation (Figure 5) predominantly reflect formation of the state $P^+Bph_A^-$. Again, the wild-type spectrum is in agreement with previously published reports (Kirmaier & Holten, 1988). Both wild-type and *syml* spectra show a bleaching of the 760-nm band due to formation of Bph^-, an apparent blue shift of the 800-nm band giving an absorbance increase near 790 nm and a decrease near 810 nm, and a bleaching of the Q_Y band of P centered at 850 nm in the wild-type and about 840 nm in the mutant. Absorption changes measured 640 ps after excitation represent $P^+Q_A^-$ formation in wild-type reaction centers (Figure 5). In both wild-type and *syml* reaction centers, these spectra correspond well to the steady-state light-induced absorbance changes in Figure 3. Room temperature measurements of the picosecond transient absorbance changes between 500 and 580 nm were also performed. Though these measurements were considerably noisier than those shown in Figure 5 and the two Bph Q_X absorption bands are poorly resolved at this temperature, there was no apparent bleaching of the Q_X band of the higher energy Bph (Bph_B) in either sample.

Comparing the short-time (0.5- or 0.8-ps) and intermediate-time (48-ps) absorption changes in Figure 5, it can be seen that in the short-time spectra between 850 and 960 nm both *syml* and wild-type display a spectral feature due to stimulated emission from P* (seen as an absorption decrease relative to the long-time spectra; Woodbury et al., 1985; Martin et al., 1986; Kirmaier & Holten, 1988). Measurements of the decay of the stimulated emission from P* at 910 nm are shown in Figure 6 for wild-type and mutant reaction centers. The calculated fit shown is the result of a global analysis assuming exponential decay kinetics over the time ranges shown between 830 and 965 nm (one kinetic trace every 2 nm). The stimulated emission from P* in wild-type reaction centers decays with a 4.3-ps time constant under the conditions of these measurements (see below) while the *syml* reaction centers yielded a 14-ps lifetime. (The error in the fitting is roughly ±5% as determined by fitting individual decay traces before summing.) The kinetics of the bleaching of the 760-nm ground state band of Bph due to $P^+Bph_A^-$ formation was also measured (data not shown). Though this signal was more noisy than that at 910 nm, the decay kinetics were similar (approximately 5 ps).

The 4.3-ps lifetime reported here for wild-type reaction centers is somewhat longer than the value reported previously (3.5 ps; Kirmaier & Holten, 1988). The measurements shown in Figures 5 and 6 were performed in a high ionic strength buffer (10 mM potassium phosphate, 0.05% LDAO, and 200 mM KCl). The *syml* reaction centers are significantly more stable for extended periods at room temperature in this buffer than in low ionic strength buffers. We have performed decay measurements of both wild-type and *syml* reaction centers at lower ionic strength [similar to that of Kirmaier and Holten (1988)] and have obtained somewhat shorter decay times for P* (3.5 ps for wild-type and 10–12 ps for *syml*).[1]

The insets in Figure 6 show the amplitude spectra associated with the exponential decay component and the constant in the global fits of the wild-type and *syml* reaction centers. The spectrum of the 4.3-ps component of wild-type reaction centers is roughly what one might expect for the stimulated emission. The spectrum of the 14-ps component of *syml* clearly includes an additional bleaching between 830 and 870 nm. In addition, there is a significant decrease in the relative level of the stimulated emission at 920 nm in *syml* reaction centers compared to that seen in wild-type reaction centers.

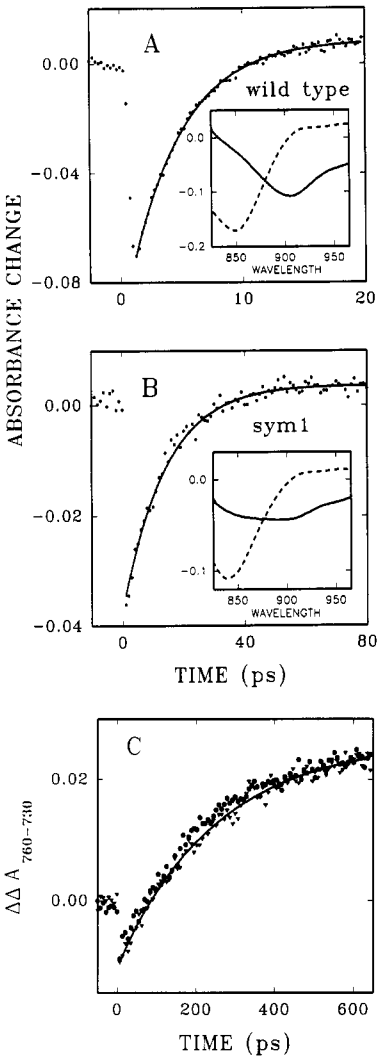

FIGURE 6: The kinetics of electron transfer in wild-type and *sym1* reaction centers. (A) Wild-type reaction centers at 910 nm. (B) *sym1* reaction centers at 910 nm. Note that the time scales for panels A and B differ by a factor of 4. The solid lines represent the results at 910 nm of a global exponential fit of the data over the entire rate vs wavelength surface (one hundred spectra at different times between 830 and 960 nm). The insets show the spectra of the amplitudes for the 4.3-ps (wild-type) or 14-ps (*sym1*) exponential decay components (solid curves) and the spectra of the constant terms (dashed curves) for the two fits. (C) Dual-wavelength absorption change measurements on the 0–640-ps time scale (760 nm minus 730 nm) for wild-type (circles) and *sym1* (triangles) reaction centers. A dual-wavelength measurement was performed in order to avoid errors due to a small base-line drift which occurs on this time scale. The data sets were normalized for comparison. (The scale shown accurately reflects the absorption changes at this wavelength in the wild-type; the absorption changes in *sym1* reaction centers were about 30% smaller.) The solid lines represent the results of a global exponential fit of the time vs wavelength surface for *sym1* reaction centers between 750 and 770 nm (11 spectral points). The time constant thus determined was 250 ps.

Longer time scale measurements of the recovery of the 760-nm Bph band as the electron is transferred from Bph_A to Q_A were also performed (Figure 6C). The 250-ps lifetime of $P^+Bph_A^-$ determined for *sym1* reaction centers was essentially the same as that found for wild-type reaction centers. Apparently there is very little change in the rate of the electron-transfer reaction from Bph_A^- to Q_A in this mutant.

The Quantum Yield of Electron Transfer. The quantum yield of $P^+Q_A^-$ formation is nearly unity in wild-type reaction centers (Feher et al., 1989). Figure 7 shows a measurement of the relative quantum yield of $P^+Q_A^-$ for *sym1* reaction centers at room temperature. The absorbance change due to

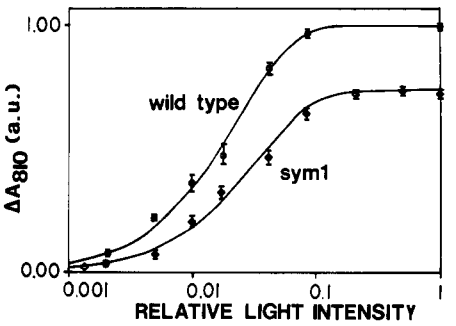

FIGURE 7: Relative quantum yield determination of $P^+Q_A^-$ in *sym1* reaction centers. The upper curve shows the relative absorbance bleaching at 810 nm induced in wild-type reaction centers by 500-ns pulses of 600-nm light of various intensities. The bottom curve is the 810-nm absorbance bleaching vs intensity for *sym1* reaction centers. Absorption bleaching is shown as a positive value for simplicity. The intensity of the excitation light was varied by calibrated neutral density filters. The solid curves represent calculated saturation curves with saturation values and half-maximal intensities chosen to best fit the data. The $P^+Q_A^-$ relative quantum yield for *sym1* reaction centers was determined from the shift in the half-maximal intensity between wild-type and *sym1* assuming a yield of 1.0 for the wild-type. The mutant and wild-type samples were used at concentrations that resulted in identical ground-state absorbance readings at 800 nm. The 25% drop in the saturation yield of $P^+Q_A^-$ in the mutant can be accounted for by considering the change in the shape of the light-minus-dark difference spectrum of *sym1* relative to wild-type (Figures 2 and 3).

P^+ formation at 810 nm was measured in both wild-type and mutant samples as a function of light intensity, and the resulting curves were analyzed assuming a homogeneous population of reaction centers in both the ground state and the state $P^+Q_A^-$. This method of determining the quantum yield of $P^+Q_A^-$ formation is independent of changes in the relative extinction coefficient at the measuring wavelength or of changes in sample concentration, though it does depend on the extinction coefficient of the active reaction centers at the excitation wavelength. Using this technique, a quantum yield for P^+ formation of approximately 70% was determined. (The error in this number due to scatter of the data and the analysis is about ±10%.) A more complete analysis of the spectral and kinetic changes associated with $P^+Q_A^-$ recombination is given in the following paper (Stocker et al., 1992).

A comparison of the spectra as a function of time for *sym1* (Figure 5B) to that for wild-type (Figure 5A) indicates that there is a substantial recovery of the bleaching in the 830–860-nm region between 2 and 50 ps in *sym1* reaction centers compared to wild-type. Analysis of these measurements can be used to estimate the yield of electron transfer between P^* and Bph_A and between Bph_A^- and Q_A (Kirmaier et al., 1988). A more quantitative picture of this situation is given in the insets to Figure 6. In wild-type, one can see that at about 838 nm the amplitude spectrum of the 4.3-ps component crosses

[1] In addition to the effects of ionic strength, variation was noted in the initial electron-transfer rate in different preparations of *sym1* reaction centers (all wild-type reaction center preparations yielded a 3.5-ps decay of P^* at low ionic strength). This variation was most significant in *sym1* reaction centers isolated from an antennaless strain of *Rb. capsulatus* (Bylina et al., 1988b). One significant difference between the preparations from B875 antenna-containing and antennaless strains was the apparent loss of Q_B when reaction centers were isolated from B875 antenna-containing strains. The variation in the decay of P^* was from 10–12 ps (B875 antenna-containing strain) to 18 ps (antennaless strain) in *sym1* reaction centers. For all the fast transient absorption measurements reported in this work, reaction centers isolated from the B875-containing strain were used at an ionic strength of about 200 mM. Many of the other experiments were performed on both samples, and no other significant differences have been detected.

Scheme I

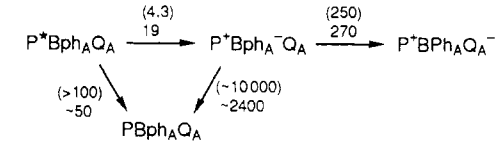

zero. If one makes the assumption that the spectral characteristics of P* and the charge-separated state formed from P* (presumably $P^+Bph_A^-$) in *syml* reaction centers are roughly the same as those observed in wild-type reaction centers, then the recovery of the bleaching seen in *syml* reaction centers at 838 nm should be due to recovery of the ground-state absorption of the Q_Y band of P. With this assumption, the fitting amplitudes at this wavelength imply that there is a 25% ground-state recovery (a 75% yield of charge separation) during the electron-transfer step from P* to $P^+Bph_A^-$. There is also a 5–10% ground-state recovery (90–95% yield of electron transfer) during the second electron-transfer step, as can be seen by comparing the 48- and 640-ps absorption change spectra in Figure 5A. This results in an overall yield of electron transfer to $P^+Q_A^-$ of 65–70%, in agreement with the long-time yield of $P^+Q_A^-$ measured by statistical curve analysis (Figure 7).

KINETIC ANALYSIS

Model-Dependent Calculations of Microscopic Rate Constants. In wild-type reaction centers, the yield of electron transfer is nearly unity and the free energy gap between the initial excited single state and $P^+Bph_A^-$ is large enough so that the overall electron-transfer reaction is nearly irreversible at room temperature. Because of this, the microscopic rate constants for forward electron transfer (ignoring any possible intermediates between P* and $P^+Bph_A^-$) are essentially the same as the observed rate constants determined from transient absorption spectroscopy.

In *syml* reaction centers, the yield of both electron-transfer steps has been decreased (Figures 6 and 7). The decreased yield of electron transfer indicates a significant contribution from reaction pathways competing with productive electron transfer. From the observed yields and reaction kinetics, one can estimate the microscopic rate constants for forward electron transfer and the rate constants for the competing decay paths, as has been done previously for other mutants that show decreased electron-transfer yields (Kirmaier et al., 1988). Scheme I shows the results of such calculations for *syml* reaction centers. The numbers shown are reciprocal rate constants in picoseconds. (Wild-type values are shown in parentheses.) Note that these calculations do not include the state $P^+Bch_A^-$. Any involvement of this state in the overall electron transfer is included in the initial rate. The effect of including $P^+Bch_A^-$ on the calculation of microscopic rate constants for electron transfer has been considered by others (Bixon et al., 1991; Holzapfel et al., 1989).

In this context, it is important to note that the measurements performed in this work do not speak to the issue of the mechanism or path of the nonproductive decay of P*. The path may be direct, involving no intermediate electronic states, or it may involve electronic states of P other than the excited singlet or there may be short-lived intermediate states between P* and the ground state which involve neighboring cofactors (e.g., P^+Bch^-). The fast transient absorption measurements in this work only provide information about the fraction of reaction centers in the state P* which go on to form a metastable (>10-ps lifetime) P^+Bph^- state.

Table III: Calculated Thermodynamic Parameters[a]

sample	a_d/a_p	K_{eq}	$\Delta G°$ (meV)[b]
w.t. RCs	0.010	96	−120
syml RCs	0.058	17	−75

[a] The ratio a_d/a_p is given by

$$a_d/a_p = (\alpha_1/\tau_1)(A_2 + A_3 + A_4)/A_1$$

where α_1 is the decay time of the stimulated emission from quinone-reduced reaction centers. Multiplying by α_1/τ_1 corrects for the limited time resolution.[2] [b] The error in $\Delta G°$ due to scatter in the fluorescence amplitudes is about ±10 meV.

Model-Dependent Calculations of the Free Energy Gap between P and $P^+Bph_A^-$.* The free energy change for the reaction between P^*Bph_A and $P^+Bph_A^-$ has been determined by several methods in wild-type reaction centers [e.g., Goldstein et al. (1988), Ogrodnik et al. (1988), and Schenck et al. (1982)]. One method for determining the free energy change is to compare the initial amplitude of the long-lived fluorescence components due to back-reactions re-forming P* with the initial amplitude of the prompt fluorescence from P* (Schenck et al., 1982; Woodbury & Parson, 1984, 1986). Assuming that P* and $P^+Bph_A^-$ are in equilibrium on the time scale of the fastest component of the long-lived fluorescence (approximately 100 ps), the equilibrium constant for this electron-transfer step is simply given by the ratio of the initial amplitude of the long-lived fluorescence to the initial amplitude of the prompt fluorescence (Schenck et al., 1982; Woodbury & Parson, 1984, 1986).

Table III lists equilibrium constants and free energies for wild-type and *syml* reaction centers and chromatophores calculated assuming rapid equilibration between the states P* and $P^+Bph_A^-$ using the relationships:

$$1/K_{eq} = (a_d/a_p)$$

$$\Delta G° = -RT \ln (K_{eq})$$

Here, a_d/a_p is the ratio of the total initial amplitude of the long-lived fluorescence over the initial amplitude of the prompt fluorescence (see Table III, footnote *a*).[2] It is clear from Table III that the *syml* mutation results in a large decrease in the calculated free energy gap between P* and $P^+Bph_A^-$ compared to wild-type.

Effects of Back-Reactions on Calculated Microscopic Rate Constants. Given the small free energy gap between P* and $P^+Bph_A^-$ in *syml* reaction centers, one might question the validity of ignoring back-reactions in Scheme I. It is possible to express the forward and backward microscopic rate constants for the initial electron-transfer reaction in reaction

[2] Since the time-correlated single-proton counting apparatus has a time resolution which is not suitable for accurately determining time constants less than about 30 ps, the values of A_1 listed for wild-type and *syml* reaction centers in Table II are probably underestimates (but see Discussion). A more accurate value can be obtained by using the integrated prompt fluorescence from Table II (i.e., $A_1\tau_1$) and dividing this by the lifetime of the stimulated emission (α_1) measured by transient absorption. Thus, the value of a_d/a_p used for the calculation of $\Delta G°$ is given by

$$a_d/a_p = (A_2 + A_3 + A_4)\alpha_1/A_1\tau_1$$

In order to obtain accurate values for α_1 (the true decay time of P*) under the conditions used in these experiments, stimulated emission decays were recorded for both wild-type and *syml* reaction centers with reduced quinones. Quinone reduction resulted in a roughly 50% increase in the time constant for P* decay in wild-type reaction centers, but resulted in only a small (10%) increase in the observed P* lifetime in *syml* reaction centers.

centers in terms of observed kinetics and amplitudes from the transient absorption and fluorescence experiments. This can be accomplished by solving the rate equations for a modified version of Scheme I, which includes a back-reaction rate constant between $P^+Bph_A^-Q_A$ and $P^*Bph_AQ_A$. However, including the back-reaction in Scheme I did not alter any of the forward electron-transfer rates by more than 10%.

Including back-reactions in the calculations did explain one interesting result seen in *syml* reaction centers. The yield estimated for the second electron-transfer step in *syml* reaction centers from transient absorption measurements (90–95%; Figure 5) is significantly less than that observed in wild-type (nearly 100%; Figure 5) even though the rate of the forward electron-transfer reaction from $Bphe_A^-$ to Q_A is very similar in the two reaction centers. This is because the small equilibrium constant for the reaction $P^* \leftrightarrow P^+Bph_A^-$ in *syml* coupled with the increased calculated decay rate of P* provides an additional, competitive pathway for decay for $P^+Bph_A^-$.

DISCUSSION

This report describes *syml*, a large-scale mutation of the *pufM* gene of the *Rb. capsulatus puf* operon. The *syml* mutation was designed to make the environment of the initial electron donor much more symmetric by substituting a 51 bp fragment of the *pufM* gene with sequence from *pufL*. Nearly half of the M amino acids closest to P are encoded within this region. In the *Rb. sphaeroides* reaction center structure, this corresponds to part of the C/D interhelix region and the top of the D helix (Allen et al., 1987).

Properties of the syml Mutation. The effects of the *syml* mutation on the overall ability of reaction centers to function in the bacterial photosynthetic apparatus are relatively minor. From the fact that this mutant is still capable of photosynthetic growth, it is clear that all of the basic reaction center functions are largely intact. The pigment composition of the mutant reaction centers also appears unaltered.

However, there are significant differences between the detailed properties of *syml* reaction centers and those from the wild-type strain. The observed decay time of the initial excited singlet state of P has increased approximately 3-fold (Figure 6) due to an estimated 5-fold decrease in the microscopic rate constant for forward electron transfer between P and Bph_A (Scheme I). The overall relative quantum yield of electron transfer to Q_A has dropped to 65–70% (Figures 5–7). The quantum yield loss in this mutant is primarily in the P* to $P^+Bph_A^-$ reaction (Figures 5 and 6). There has also been a 10–15-nm blue shift of the Q_Y band of P in *syml* relative to wild-type. This can be seen in the $P^+Q_A^-$ difference spectrum of the photosynthetic membranes (Figure 2) or the spectra of the isolated reaction centers (Figure 3). Assuming that this corresponds to a shift in the zero–zero transition energy of P, then it is indicative of an increase in the energy of P* relative to the ground state of approximately 20 meV. The 1250-nm band of P^+ shifts to about 1240 nm in *syml* reaction centers; this shift is accompanied by a 4-fold decrease in oscillator strength (Figure 3). In addition, the relative extinction coefficient for stimulated emission from P* has dropped approximately 2-fold in *syml* vs wild-type. These bandshifts indicate a significant change either in the interaction between the two bacteriochlorophylls in the dimer or in the electronic environment of the special pair.

One of the striking alterations in the parameters of electron transfer in this symmetry mutant is the apparent decrease in the free energy gap between P* and $P^+Bph_A^-$. The driving force for electron transfer between P and Bph_A in quinone-reduced reaction centers has decreased from about −120 meV in the wild-type to about −75 meV in *syml* (Table III). It should be pointed out that there are potential inaccuracies associated with estimating free energy changes from time-resolved fluorescence measurements. One of these is that the method normally used to measure the fluorescence decay as a function of time (time-correlated single-photon counting) does not have sufficient time resolution to accurately resolve the initial decay of P*, at least in wild-type reaction centers. Thus, some sort of correction based on other kinetic measurements must be applied (see footnote 2). In light of recent evidence that the initial decay of P* is not a simple, single exponential process (Du et al., 1992; Vos et al., 1991), the accuracy of this correction becomes questionable. Note that for both wild-type and *syml* reaction centers the value of the decay of P* determined by single-photon counting is nearly twice that determined by pump–probe measurements of the decay of the stimulated emission. This is probably not simply a reflection of the time resolution limits of single photon counting, at least in the case of *syml* reaction centers, but instead may indicate a multiexponential decay of P* involving longer-lived components with small amplitudes, making them difficult to observe in the stimulated emission measurements, but giving them a significant effect on the overall lifetime determined in the time-correlated single-photon counting experiments.

However, correcting for these effects would not change the overall qualitative conclusion that the driving force for electron transfer from P* to $P^+Bph_A^-$ is significantly decreased in *syml* reaction centers vs wild-type. In fact, the nonexponential behavior of the P* decay in both wild-type and *syml* reaction centers would tend to simply shift the free energy differences estimated for both samples in the same direction.

These findings prompt the following question: What are the specific molecular interactions that have been altered in *syml* which give rise to the change in the free energy gap between P* and $P^+Bph_A^-$? In the following paper (Stocker et al., 1992), it was shown that the major contribution to this change in ΔG° is a dramatic increase in the potential of the P/P^+ redox couple. The molecular mechanism responsible for this change will be investigated by demonstrating that many of the properties of the *syml* mutation, including the change in the redox potential of P, arise from the replacement of a single M amino acid (M195) by its L counterpart.

The Effect of the syml Mutation on the Intrinsic Rate of P Decay.* The 5-fold decrease in the microscopic forward rate constant for electron transfer from P to Bph_A is not too surprising given the apparent decrease in the driving force for this reaction. What is more surprising is the apparent increase in the rate of the intrinsic decay of P*. According to most reports, the quantum yield of electron transfer from P* to Q_A in wild-type reaction centers is greater than 0.95. If one assumes that the yield of the Bph_A^- to Q_A electron-transfer step is roughly 0.98 (calculated from the 200-ps electron-transfer time at this step and the 10–15-ns recombination time of $P^+Bph_A^-$ when Q_A is reduced or removed), this implies that the yield at the first step is at least 0.97. From this, one can estimate that the competing intrinsic decay rate of P* to the ground state in wild-type reaction centers has a reciprocal rate constant slower than $(100\ ps)^{-1}$. This is in agreement with the measured P* decay times in a mutant that does not undergo electron transfer (190 ps; Breton et al., 1990) and *Rb. sphaeroides* reaction centers which have both Q_A and Bph_A reduced (350 ps; Schenck et al., 1981), as well as with estimates of the intrinsic P* decay times made by others (>150

ps; McDowell et al., 1990; Nagarajan et al., 1990). Thus, the 50-ps intrinsic P* decay time determined for *syml* reaction centers is at least 2-fold faster than the wild-type rate.

A similar situation has been found in the His to Leu mutation at M200 in *Rb. capsulatus* which is known as the heterodimer mutant (Kirmaier et al., 1988; McDowell et al., 1990, 1991). In this mutant, the initial electron donor (referred to as "D") is a heterodimer of Bch and Bph. The calculated D* to Bph_A electron-transfer time in this mutant is increased to about 30 ps, and the intrinsic decay time of the heterodimer excited state is about 30 ps. The increased intrinsic decay of D* in this mutant has been attributed either to a low-energy intradimer charge-transfer state which mixes very strongly into D* or to an intradimer charge-separated state which is formed very rapidly from D* (Kirmaier et al., 1989; McDowell et al., 1990, 1991). It is possible that in *syml* reaction centers the energy of an intradimer charge transfer state is lower than in wild-type reaction centers. However, unlike the heterodimer mutant, stimulated emission from P* is observed in *syml* reaction centers (though it is weaker than that in wild-type), indicating that the excited state is not rapidly converted to a nonemitting state nor is P* a nonemitting state in the 900–950-nm region. Future experiments on *syml* and related mutants will include attempting to directly observe an anion band associated with Bch^- in the 600–700-nm region corresponding to a major contribution from a charge-transfer or charge-separated intradimer state at early times (Kirmaier et al., 1989; McDowell et al., 1990). Measurements of the Stark effect on the low-temperature absorption spectrum also address this issue and are presented in the following paper.

Role of Protein Symmetry/Asymmetry in Reaction Center Function. One major question left unanswered by this work is whether there is any increase in the amount of electron transfer along the B-side electron-transfer pathway in this mutant. Bph_A and Bph_B have slightly different transition energies in their Q_X bands which are well enough resolved at low temperature to quantitate the relative amounts of Bph_A anion and Bph_B anion formed on the picosecond time scale (Kirmaier & Holten, 1989). However, the spectral resolution of the room temperature transient absorption measurements in the 500–580-nm region reported here is insufficient to make an accurate estimate of electron transfer to Bph_B. Qualitatively, no significant difference was observed between wild-type and *syml* absorbance change spectra in this region, indicating that the major product formed on the 50-ps time scale is $P^+Bph_A^-$. This is consistent with the quantum yield analysis, which indicates that almost all of the reaction centers which formed a metastable P^+Bph^- state went on to form $P^+Q_A^-$. Obviously, the issue of electron-transfer asymmetry was a major motivation in the design of the *syml* mutation, and more quantitative measurements designed to address this question are being pursued.

One can say something more general about the relationship between reaction center function and the symmetry of the environment near the special pair from this work and related work by others. Extrapolating from the *Rb. sphaeroides* reaction center structure to the structure expected for *Rb. capsulatus* reaction centers, there are approximately 11 amino acids in the M subunit that come close enough to P to have profound effects on its environment and are not identical to their counterparts in the L subunit (Table IV; El-Kabbani et al., 1991; Yeates et al., 1988). Five of these amino acids are between M187 and M203 (the segment exchanged in *syml*). These are M187 (Phe to Thr), M188 (Ser to Gly), M194 (Leu to Phe), M195 (Phe to His), and M203 (Ser to Gly)

Table IV: Amino Acids near P

M amino acids in vicinity of P					homologous L amino acids[b]			
no.	*caps*	*sph*	*vir*	*syml*	*caps*	*sph*	*vir*	no.
M154	Leu	Leu	Phe	Leu	Ala	Ala	Met	L127
M184	Thr	Thr	Leu	Thr	Val	Val	Val	L157
M187	**Phe**	**Phe**	**Phe**	**Thr**	**Thr**	**Thr**	**Phe**	**L160**
M188	**Ser**	**Ser**	**Ser**	**Gly**	**Gly**	**Gly**	**Gly**	**L161**
M194	**Leu**	**Leu**	**Phe**	**Phe**	**Phe**	**Phe**	**Trp**	**L167**
M195	**Phe**	**Phe**	**Tyr***	**His**	**His**	**His***	**His***	**L168**
M203	**Ser**	**Ser**	**Ser**	**Gly**	**Gly**	**Ala**	**Ser**	**L176**
M207	Leu	Leu	Ala	Leu	Phe	Phe	Leu	L180
M208	Tyr	Tyr	Tyr	Tyr	Phe	Phe	Phe	L181
M278	Gly	Gly	Ala	Gly	Ser	Ser	Gly	L244
M282	Ile	Ile	Ile	Ile	Met	Met	Thr*	L248

[a] Amino acids in the *syml* region are indicated in bold. *caps*: *Rb. capsulatus*; *sph*: *Rb. sphaeroides*; *vir*: *Rps. viridis*; *: amino acids involved in H-bonds (El-Kabbani et al., 1991; Yeates et al., 1988). The amino acid alignment used was that of Michel et al. (1986). [b] The L subunit amino acids which are symmetry-related to the listed M subunit amino acids are shown.

(Figure 1). The remaining six amino acids are Leu M154 (its counterpart in L is an Ala), Thr M184 (Val in L), Leu M207 (Phe in L), Tyr M208 (Phe in L), Gly M278 (Ser in L), and Ile M282 (Met in L). M208 has been changed to its L counterpart by other researchers (Nagarajan et al., 1990; Finkele et al., 1990). This also resulted in a significant decrease in the forward rate constant for electron transfer from P to Bph_A at room temperature, but produced an otherwise functional reaction center. Of the remaining four residues, M207 was part of a much larger symmetry mutant produced by Youvan and co-workers (Robles et al., 1990). This mutant alters amino acids near several reaction center cofactors and apparently results in loss of Bph_A. However, single-site revertants have been isolated that grow photosynthetically and still contain the Leu to Phe conversion at M207. Thus, it is possible, at least in certain groupings, to symmetrize 7 of the 11 amino acids most closely associated with P without losing overall reaction center function.

One can expand this analysis of symmetry requirements in the vicinity of P by considering species variation. Table IV gives the amino acids at the positions in the M and L subunits of *Rb. capsulatus*, *Rb. sphaeroides*, and *Rhodopseudomonas viridis* reaction centers corresponding to the 11 amino acids identified above as being in the vicinity of P. There are four cases where all three species clearly show functionally nonconservative changes between the L and M subunits. These are M188 (Ser vs Gly in all species), M195 (Phe or Tyr vs His), M208 (Tyr vs Phe in all species), and M282 (Ile vs Met or Thr). Three of these M amino acids have been replaced by their L counterparts in this work or in work by others. Thus, with the exception of M282, either all of the amino acids which make up the immediate environment of the special pair have been replaced on the M side by their L counterparts without overall loss of reaction center function or the difference between the amino acids on the two sides is a relatively conservative one in some species. It appears that asymmetry in the vicinity of P, though important in optimizing the rate and yield of initial electron transfer, is not a strict requirement for the overall function of the photosynthetic bacterial reaction center.

ACKNOWLEDGMENT

We thank Drs. James Allen and JoAnn Williams for many useful discussions and for critical reading of the manuscript.

REFERENCES

Allen, J. P., Feher, G., Yeates, T. O., Rees, D. C., Deisenhofer, J., Michel, H., & Huber, R. (1987) *Proc. Natl. Acad. Sci. U.S.A. 84*, 5730–5734.

Bixon, M., Jortner, J., & Michel-Beyerle, M. E. (1991) *Biochim. Biophys. Acta 1056*, 301–315.

Breton, J., Martin, J.-L., Lambry, J.-C., Robles, S. J., & Youvan, D. C. (1990) in *Reaction Centers of Photosynthetic Bacteria* (Michel-Beyerle, M. E., Ed.) pp 293–302, Springer Verlag, Berlin, Germany.

Bylina, E. J., Ismail, S., & Youvan, D. C. (1986) *Plasmid 16*, 175–181.

Bylina, E., Kirmaier, C., McDowell, L. M., Holten, D., & Youvan, D. C. (1988a) *Nature 336*, 182–184.

Bylina, E. J., Robles, S. J., & Youvan, D. C. (1988b) *Israel J. Chem. 28*, 73–78.

Chan, C.-K., Chen, L. X.-Q., DiMagno, T. J., Hanson, D. K., Nance, S. L., Schiffer, M., Norris, J. R., & Fleming, G. R. (1991) *Chem. Phys. Lett. 176*, 366–372.

Chang, C.-H., El-Kabbani, O., Tiede, D., Norris, J., & Schiffer, M. (1991) *Biochemistry 30*, 5352–5360.

Deisenhofer, J., Epp, O., Miki, K., Huber, R., & Michel, H. (1984) *J. Mol. Biol. 180*, 385–398.

Du, M., Rosenthal, S. J., Xie, X., DiMagno, T. J., Schmidt, M., Norris, J. R., & Fleming, G. R. (1992) *Proc. Natl. Acad. Sci. U.S.A.* (in press).

El-Kabbani, O., Chang, C.-H., Tiede, D., Norris, J., & Schiffer, M. (1991) *Biochemistry 30*, 5361–5369.

Farchaus, J. W., & Oesterhelt, D. (1989) *EMBO J. 8*, 47–54.

Feher, G., Allen, J. P., Okamura, M. Y., & Rees, D. C. (1989) *Nature 339*, 111.

Finkele, U., Lauterwasser, L., Zinth, W., Gray, K. A., & Oesterhelt, D. (1990) *Biochemistry 29*, 8517.

Goldstein, R. A., Takiff, L., & Boxer, S. G. (1988) *Biochim. Biophys. Acta 934*, 253–263.

Gust, D., Moore, T. A., Luttrull, D. K., Seely, G. R., Bittersmann, E., Bensasson, R. V., Rougee, M., Land, E. J., De Schryver, F. C., & Van der Auweraer, M. (1990) *Photochem. Photobiol. 51*, 419–426.

Hammes, S. L., Mazzola, L., Boxer, S. G., Gaul, D. F., & Schenck, C. C. (1990) *Proc. Natl. Acad. Sci. U.S.A. 87*, 5682–5686.

Holzapfel, W., Finkele, U., Kaiser, W., Oesterhelt, D., Scheer, H., Stilz, H. U., & Zinth, W. (1989) *Chem. Phys. Lett. 160*, 1–7.

Kirmaier, C., & Holten, D. (1987) *Photosynth. Res. 13*, 225–260.

Kirmaier, C., & Holten, D. (1988) *Israel J. Chem. 28*, 79–85.

Kirmaier, C., Holten, D., Bylina, E. J., & Youvan, D. C. (1988) *Proc. Natl. Acad. Sci. U.S.A. 85*, 7562–7566.

Kirmaier, C., Bylina, E. J., Youvan, D. C., & Holten, D. (1989) *Chem. Phys. Lett. 159*, 251–257.

Kirmaier, C., Gaul, D., DeBey, R., Holten, D., & Schenck, C. (1991) *Science 251*, 922–927.

Martin, J. L., Breton, J., Hoff, A. J., Migus, A., & Antonetti, A. (1986) *Proc. Natl. Acad. Sci. U.S.A. 83*, 957–961.

McDowell, L. M., Kirmaier, C., & Holten, D. (1990) *Biochim. Biophys. Acta 1020*, 239–246.

McDowell, L. M., Kirmaier, C., & Holten, D. (1991) *J. Phys. Chem. 95*, 3379–3383.

Michel, H., Weyer, K. A., Gruenberg, H., Dunger, I., Oesterhelt, D., & Lottspeich, F. (1986) *EMBO J. 5*, 1149–1158.

Middendorf, T. R., Mazzola, L. T., Gaul, D. F., Schenck, C. C., & Boxer, S. G. (1991) *J. Phys. Chem. 95*, 10142–10151.

Nagarajan, V., Parson, W. W., Gaul, D., & Schenck, C. C. (1990) *Proc. Natl. Acad. Sci. U.S.A. 87*, 7888–7892.

Ogrodnick, A., Volk, M., Letterer, R., Feick, R., & Michel-Beyerle, M. E. (1988) *Biochim. Biophys. Acta 936*, 361–371.

Paddock, M. L., Rongey, S. H., Feher, G., & Okamura, M. L. (1989) *Proc. Natl. Acad. Sci. U.S.A. 86*, 6602.

Prince, R. C., & Youvan, D. C. (1987) *Biochim. Biophys. Acta 890*, 286–291.

Robles, S. J., Breton, J., & Youvan, D. C. (1990) *Science 248*, 1402–1405.

Schenck, C. C., Parson, W. W., Holten, D., & Windsor, M. W. (1981) *Biochim. Biophys. Acta 635*, 383–392.

Schenck, C. C., Blankenship, R. E., & Parson, W. W. (1982) *Biochim. Biophys. Acta 680*, 44–59.

Sebban, P., & Moya, I. (1983) *Biochim. Biophys. Acta 722*, 436–442.

Simon, R., Priefer, U., & Puhler, A. (1983) *Bio/Technology 1*, 784–791.

Stocker, J. W., Taguchi, A. K. W., Murchison, H. A., Woodbury, N. W., & Boxer, S. G. (1992) *Biochemistry* (following paper in this issue).

Takahashi, E., Maroti, P., & Wraight, C. A. (1990) in *Current Research in Photosynthesis* (Baltscheffsky, M., Ed.) Vol. 1, p 172, Kluwer Academic Publishers, Boston, MA.

van der Rest, M., & Gingras, G. (1974) *J. Biol. Chem. 249*, 6446–6453.

Vos, M. H., Lambry, J. C., Robles, S. J., Youvan, D. C., Breton, J., & Martin, J.-L. (1991) *Proc. Natl. Acad. Sci. U.S.A. 88*, 8885–8889.

Williams, J., Murchison, H. A., Woodbury, N. W., Alden, R. G., Taguchi, A. K. W., & Allen, J. P. (1992) *Biochemistry* (in press).

Woodbury, N. W. T., & Parson, W. W. (1984) *Biochim. Biophys. Acta 767*, 345–361.

Woodbury, N. W., & Parson, W. W. (1986) *Biochim. Biophys. Acta 850*, 197–210.

Woodbury, N. W., Becker, M., Middendorf, D., & Parson, W. W. (1985) *Biochemistry 24*, 7516–7521.

Woodbury, N. W., Taguchi, A. K., Stocker, J. W., & Boxer, S. G. (1990) in *Reaction Centers of Photosynthesis Bacteria* (Michel-Beyerle, M. E., Ed.) pp 303–312, Springer Verlag, Berlin, Germany.

Yeates, T. O., Komiya, H., Chirino, A., Rees, D. C., Allen, J. P., & Feher, G. (1988) *Proc. Natl. Acad. Sci. U.S.A. 85*, 7993–7997.

Youvan, D. C., Ismail, S., & Bylina, E. J. (1985) *Gene 38*, 19–30.